

# Ultrabroadband Red Luminescence of Mn<sup>4+</sup> in Spinel Peaking at 651 nm

Haipeng Ji,<sup>1</sup> Xinghui Hou,<sup>1</sup> Maxim S. Molokeev,<sup>2,3</sup> Jumpei Ueda,<sup>4</sup> Setsuhisa Tanabe,<sup>4</sup> Mikhail G. Brik,<sup>5,6</sup> Zongtao Zhang,<sup>1</sup> Yu Wang,<sup>1,\*</sup> Deliang Chen<sup>1,\*</sup>

1 School of Materials Science and Engineering, Zhengzhou University, Zhengzhou 450001, China

2 Laboratory of Crystal Physics, Kirensky Institute of Physics, Federal Research Center KSC SB RAS, Krasnoyarsk 660036, Russia

3 Siberian Federal University, Krasnoyarsk 660041, Russia

4 Graduate School of Human and Environmental Studies, Kyoto University, Kyoto 606-8501, Japan

5 CQUPT-BUL Innovation Institute & College of Sciences, Chongqing University of Posts and Telecommunications, Chongqing 400065, China

6 Institute of Physics, University of Tartu, Tartu 50411, Estonia

## Corresponding authors:

Yu Wang (wangyu@zzu.edu.cn), Deliang Chen (dlchen@zzu.edu.cn)

## Abstract

Blue light pumped red luminescence with broadband and high photon-energy emission is highly desired for phosphor-converted white light-emitting diodes (LEDs), to achieve high color rendering index and high luminous efficacy. The Mn<sup>4+</sup>-doped red-emitting phosphors generally exhibit sharp vibronic emissions associated with the parity and spin-forbidden <sup>2</sup>E<sub>g</sub> → <sup>4</sup>A<sub>2g</sub> transition. Herein, we report the MgAl<sub>2</sub>O<sub>4</sub>:Mn<sup>4+</sup> phosphor with high photon-energy emission peaking at 651 nm in which two abnormal luminescence behaviors were observed. Firstly, the Mn<sup>4+</sup> <sup>2</sup>E<sub>g</sub> → <sup>4</sup>A<sub>2g</sub> transition exhibited ultrabroadband luminescence band in the MgAl<sub>2</sub>O<sub>4</sub> spinel and the large full-width at half-maximum (FWHM) showed dependence both on the calcination temperature as well as the partial substitution of Al<sup>3+</sup> by Ga<sup>3+</sup>. Secondly, the thermal quenching behavior of the Mn<sup>4+</sup> <sup>2</sup>E<sub>g</sub> → <sup>4</sup>A<sub>2g</sub> luminescence in MgAl<sub>2</sub>O<sub>4</sub> showed dependence on the preparation (thermal history and method of preparation). By means of Rietveld refinement and Raman technique, we demonstrate that such variation of the PL FWHM is a sum effect of structural ordering (isotropic displacement decrease of constituent atoms) and the Mg ↔ Al antisite disorder. A model for the observed varying thermal quenching of luminescence was also tentatively proposed. The results give a new perspective to understand the luminescence spectra of Mn<sup>4+</sup> <sup>2</sup>E<sub>g</sub> → <sup>4</sup>A<sub>2g</sub> transition.

**Keywords** Mn<sup>4+</sup>, Luminescence, Spinel, Antisite disorder, Thermal quenching

# 1 Introduction

The dominating phosphor-converted white Light-Emitting Diodes (pc-wLEDs) which combine the blue-emitting LED and yellow-emitting phosphor (such as  $\text{Y}_3\text{Al}_5\text{O}_{12}:\text{Ce}^{3+}$ ) generate cool white light with relatively high correlated color temperature (CCT > 4500 K) and low color rendering index (CRI;  $R_a < 80$ ) due to the lack of red component.<sup>1</sup> In the last decade,  $3.5\text{MgO}\cdot 0.5\text{MgF}_2\cdot \text{GeO}_2:\text{Mn}^{4+}$  has been commercially employed as a red phosphor in fluorescent lamp. Since the commercialization of  $\text{Mn}^{4+}$  activated fluoride phosphors (typically  $\text{K}_2\text{SiF}_6:\text{Mn}^{4+}$ ) in blue LED pumped white lighting,<sup>2</sup>  $\text{Mn}^{4+}$  has been intensively studied as a blue-to-red converting ion for LED phosphors. The spin-allowed  $\text{Mn}^{4+} {}^4\text{A}_{2g} \rightarrow {}^4\text{T}_{2g}$  transition can be excited by blue LED avoiding cascade reabsorption of yellow light from the yellow-emitting phosphor, and the manganese is more abundant than the rare earth ( $\text{Eu}^{2+}$ ,  $\text{Ce}^{3+}$ , *etc.*) which would help lower the production cost of red phosphors.<sup>3</sup>

$\text{Mn}^{4+}$  ( $3d^3$  electron configuration) prefers to get stabilized in octahedral symmetry with the three d electrons occupying the three low-lying  $t_{2g}$  orbitals split by the octahedral field. The  $\text{MgAl}_2\text{O}_4$  spinel is a typical host containing  $[\text{AlO}_6]$  octahedra.  $\text{Mg}^{2+}$  and  $\text{Al}^{3+}$  sit in the tetrahedral (1/8 occupied) and octahedral (1/2 occupied) sites, respectively. The  $\text{MgAl}_2\text{O}_4$  can perfectly accommodate  $\text{Mn}^{4+}$ , as the effective ion radius of the six-fold coordinated  $\text{Al}^{3+}$  ( $r = 0.535 \text{ \AA}$ ) is close to that of  $\text{Mn}^{4+}$  ( $r = 0.530 \text{ \AA}$ ). The  $\text{MgAl}_2\text{O}_4$  also holds a high Debye temperature of 776 K (for single crystal)<sup>4</sup>, suggesting a quite rigid crystal lattice. Although a number of aluminates have been studied as hosts for  $\text{Mn}^{4+}$  such as  $\text{SrAl}_{12}\text{O}_{19}$ ,  $\text{Sr}_4\text{Al}_{14}\text{O}_{25}$ ,  $\text{SrAl}_4\text{O}_7$ , *etc.*, our as-prepared  $\text{MgAl}_2\text{O}_4:\text{Mn}^{4+}$  shows luminescence with very short wavelength peaking at 651 nm, which is the shortest peak wavelength of the  $\text{Mn}^{4+} {}^2\text{E}_g \rightarrow {}^4\text{A}_{2g}$  transition that has ever been observed in  $\text{Mn}^{4+}$ -doped aluminates. Table 1 lists a number of  $\text{Mn}^{4+}$ -doped aluminate phosphors; the shortest emission wavelength of  $\text{Mn}^{4+}$  that has been achieved in oxide is seen to be 652 nm in either  $\text{Sr}_4\text{Al}_{14}\text{O}_{25}$  or  $\text{Sr}_2\text{Al}_6\text{O}_{11}$ . Furthermore, typical  $\text{Mn}^{4+}$ -doped red-emitting phosphors, for example, the  $\text{K}_2\text{SiF}_6:\text{Mn}^{4+}$  phosphor, tend to exhibit sharp vibronic emissions from the *intraconfigurational* parity- and spin-forbidden  ${}^2\text{E}_g \rightarrow {}^4\text{A}_{2g}$  transition. However, the full-width at half-maximum (FWHM) of the as-prepared  $\text{MgAl}_2\text{O}_4:\text{Mn}^{4+}$  is relatively quite large. The high photon-energy emission and the large FWHM of  $\text{MgAl}_2\text{O}_4:\text{Mn}^{4+}$  would benefit for a relatively high luminous efficacy and high color rendering index for pc-wLEDs. As indicated from

the Tanabe-Sugano diagram for a  $d^3$  ion<sup>5</sup>, the luminescence would exhibit broad band when the ion is experiencing a weak crystal field from the spin-allowed  ${}^4T_{2g} \rightarrow {}^4A_{2g}$  transition while it will exhibit sharp emission peaks in a strong crystal field from the spin-forbidden  ${}^2E_g \rightarrow {}^4A_{2g}$  transition. Due to a high effective positive charge,  $Mn^{4+}$  tends to experience a large crystal field strength and only transition from the  ${}^2E_g$  level is expected. Thus, the origin of the broadband emission observed for  $MgAl_2O_4:Mn^{4+}$  remains to be verified.

In this paper, we prepared  $MgAl_2O_4:Mn^{4+}$  using the co-precipitation method. The precursor was treated at 700-1300 °C to control the anti-site disorder degree so that its effect on the luminescence can be studied. The temperature-dependent luminescence intensity and the zero phonon line (ZPL) emission of  $MgAl_2O_4:Mn^{4+}$  were characterized for the first time. Moreover, we report our findings on the correlation between the unusual large FWHM and the anti-site defect as well as the isotropic displacement of constituent atoms in  $MgAl_2O_4:Mn^{4+}$  phosphor, revealing the intrinsic reason for the ultrabroadband emission of  $Mn^{4+} {}^2E_g \rightarrow {}^4A_{2g}$  transition. The thermal quenching behavior of the  $Mn^{4+} {}^2E_g \rightarrow {}^4A_{2g}$  luminescence was also found to be abnormal, which depends on the thermal history. Such findings could be inspiring for the development of new  $Mn^{4+}$ -activated broadband and thermally robust red-emitting phosphors for blue LED pumped white lighting.

**Table 1**  $Mn^{4+}$ -doped aluminate phosphors and the corresponding peaking emission

No.	Phosphor	Peak wavelength	No.	Phosphor	Peak wavelength
1	$Sr_4Al_{14}O_{25}:Mn^{4+}$	652 nm <sup>6,7</sup>	11	$Y_3Al_5O_{12}:Mn^{4+}$	670 nm <sup>8</sup>
2	$Sr_2Al_6O_{11}:Mn^{4+}$	652 nm <sup>9</sup>	12	$CaY_2Al_4SiO_{12}:Mn^{4+}$	674 nm <sup>10</sup>
3	$SrAl_{12}O_{19}:Mn^{4+}$	655 nm <sup>11</sup>	13	$Al_2O_3:Mn^{4+}$	676 nm <sup>12</sup>
4	$CaMg_2Al_{16}O_{27}:Mn^{4+}$	655 nm <sup>13</sup>	14	$YAlO_3:Mn^{4+}$	697 nm <sup>14</sup>
5	$SrAl_4O_7:Mn^{4+(*)}$	656 nm <sup>15</sup>	15	$GdAlO_3:Mn^{4+}$	698 nm <sup>16</sup>
6	$CaAl_4O_7:Mn^{4+(*)}$	656 nm <sup>17</sup>	16	$CaYAlO_4:Mn^{4+}$	710 nm <sup>18</sup>
7	$Sr_2MgAl_{22}O_{36}:Mn^{4+}$	658 nm <sup>19</sup>	17	$LaAlO_3:Mn^{4+}$	712 nm <sup>20</sup>
8	$CaAl_{12}O_{19}:Mn^{4+}$	658 nm <sup>21</sup>	18	$LiAl_5O_8:Mn^{4+}$	714 nm <sup>22</sup>
9	$SrMgAl_{10}O_{17}:Mn^{4+}$	660 nm <sup>23</sup>	19	$Ca_{14}Al_{10}Zn_6O_{35}:Mn^{4+}$	715 nm <sup>24</sup>
10	$ZnAl_2O_4:Mn^{4+}$	666 nm <sup>25</sup>	20	$SrLaAlO_4:Mn^{4+}$	715 nm <sup>26</sup>

(\*) These compounds do not consist of octahedral coordination.

## 2 Experimental and computational methods

### 2.1 Preparation

The phosphors with nominal composition of  $\text{MgAl}_{2-x}\text{Mn}_x\text{O}_4$  ( $x = 0.002$ ) were synthesized by the co-precipitation method.<sup>27</sup>  $\text{MgCl}_2 \cdot 6\text{H}_2\text{O}$  (A.R., Sinopharm),  $\text{Al}(\text{NO}_3)_3 \cdot 9\text{H}_2\text{O}$  (A.R., Sinopharm) and  $\text{Mn}(\text{NO}_3)_2$  (50 wt% solution, Aladdin) were used as raw chemicals, and ammonia water ( $\text{NH}_4\text{OH}$  28%, Sinopharm) were used as the precipitating agent. A metal nitrate solution, which contains 20 mmol of  $\text{Al}^{3+}$ , 10 mmol of  $\text{Mg}^{2+}$  and  $10x$  mmol of  $\text{Mn}^{2+}$ , was prepared by dissolving the raw nitrates into 50 ml deionized water. Then, the metal nitrate solution was added dropwise into 50 mL ammonia water under magnetic stirring. White precipitates appeared instantly upon mixing. The pH of the resultant suspension was around 10. Next, the suspension was aged at 75 °C for 1 h in a water bath. After aging, the solid in the suspension was concentrated by centrifugation at 5000 r/min for 5 min, and then dried at 110 °C for 12 h. The obtained precursor showed light pink color and was quite glutinous. Thus, without grinding, the precursor was heated at 450 °C for 3 h (at this temperature, nucleation of  $\text{MgAl}_2\text{O}_4$  starts<sup>28</sup>), thoroughly ground, and finally sintered for 3 h at 700 °C, 1000 °C, or 1300 °C, respectively. All the heat treatments were conducted in air. [Figure 1a](#) illustrates the procedure.

Furthermore, to chemically introduce the anti-site disorder, some  $\text{Al}^{3+}$  in  $\text{MgAl}_2\text{O}_4$  were substituted by  $\text{Ga}^{3+}$ , and the solid solution phosphors with nominal compositions of  $\text{MgAl}_{2-y}\text{Ga}_y\text{O}_4:0.002\text{Mn}^{4+}$  ( $y = 0, 0.5, 1.0$ ) were prepared by the high-temperature solid state reaction. The stoichiometric ratios of  $\text{MgO}$ ,  $\text{Al}_2\text{O}_3$ ,  $\text{Ga}_2\text{O}_3$  and  $\text{MnCO}_3$  chemicals (all A.R. grade) were weighed and mixed in an agate mortar, which were then preheated at 450 °C for 3 h and finally heated at 1550 °C for 6 h. The products were pulverized into fine powder prior to optical measurements.

### 2.2 Characterization

The X-ray diffraction (XRD) patterns were collected on an X-ray diffractometer (DX-2700BH, DanDong Haoyuan Instrument Co. Ltd, Liaoning, China) using  $\text{Cu-K}\alpha 1$  radiation with operating voltage and current of 40 kV and 30 mA, respectively. The XRD patterns for phase identification and for Rietveld refinement were collected in the  $2\theta$  range of 10-80° (step 0.02°, exposition time 0.2 s

per step) and 10-120° (step 0.02°, exposition time 1.5 s per step), respectively. The photoluminescence excitation (PLE) spectra were measured by the Spectrofluorometer (FluoroMax-4, Horiba Jobin Yvon, France). The temperature-dependent photoluminescence emission (PL) was measured in the temperature range of 100 K to 470 K using the setup as described previously<sup>29</sup>, which consists of a multichannel charge-coupled device (QE65Pro, Ocean Optics, USA) and a thermal stage (10033L, Linkham, UK); a 440 nm laser diode with a 550 nm short-cut filter was employed as the excitation source. The morphology was observed on a scanning electron microscope (SEM; TM3030Plus Tabletop, Hitachi, Japan). The powder sample was ultrasonically dispersed into ethanol to form a suspension which was dropped on a silicon plate. The Raman spectra were collected on a LabRAM HR Evolution spectrometer (Horiba Jobin Yvon, France) at room temperature, using the 532 nm laser light as an excitation source.

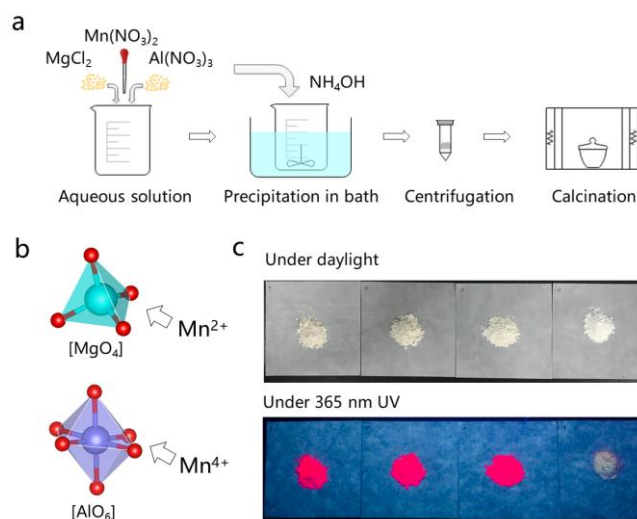


**Figure 1** (a) Synthesis flow chart, (b) the  $[MgO_4]$  tetrahedron and  $[AlO_6]$  octahedron in  $MgAl_2O_4$  which can accommodate manganese as  $Mn^{2+}$  or  $Mn^{4+}$ , (c) digital image of the  $MgAl_2O_4:Mn$  phosphors under daylight or 365 nm UV irradiation (from left to right: the calcination schedule is 700 °C×3 h, 1000 °C×3 h, 1300 °C×3 h, and 1400 °C×12 h, respectively). The difference in color is related to different absorption properties of the phosphors, which originates from the distribution of  $Mn^{4+/2+}$  in  $[AlO_6]$  or  $[MgO_4]$ .

### 2.3 Computational details

The energy levels of the  $Mn^{4+}$  ions in  $MgAl_2O_4$  were theoretically calculated using the exchange

charge model. The crystal structural data of  $\text{MgAl}_2\text{O}_4$  were used to analyze the symmetry properties of the impurity ion site and generate a cluster consisting of 62 210 ions (this is needed to ensure proper convergence of the crystal lattice sums needed for the calculations of the crystal field parameters). Details of the calculations as well as all relevant equations can be found in related ref.<sup>20, 30, 31, 32</sup> and are not repeated for the sake of brevity.

### 3 Results and discussion

#### 3.1 Phase formation and the selective occupation of the manganese dopant

The structure of  $\text{MgAl}_2\text{O}_4$  comprises both  $[\text{MgO}_4]$  tetrahedra and  $[\text{AlO}_6]$  octahedra, which accommodate the manganese either as  $\text{Mn}^{2+}$  or  $\text{Mn}^{4+}$  (illustrated in Figure 1b).  $\text{Mn}^{4+}$  with  $3d^3$  electron configuration gets stabilized when doped in the  $[\text{AlO}_6]$  octahedron. The samples calcined at 700, 1000 or 1300 °C for 3 h show the body color of light pink and emit red when irradiated by 365 nm, while the one calcined at 1400 °C for 12 h appears white and emits green under 365 nm UV (shown in Figure 1c). This evidences that the manganese was firstly doped into the six-fold coordinated  $\text{Al}^{3+}$  site as  $\text{Mn}^{4+}$ , and then under higher temperature and longer duration, was promoted to occupy the four-fold coordinated  $\text{Mg}^{2+}$  site as  $\text{Mn}^{2+}$ . This result contributes new knowledge on the selective occupation of manganese in  $\text{MgAl}_2\text{O}_4$ , in addition to that revealed by Wakui *et al.*<sup>33</sup> (that is, excessive-MgO in starting materials favors the substitution of  $\text{Mn}^{4+}$  in octahedral site while deficient-MgO leads to substitution of  $\text{Mn}^{2+}$  in tetrahedral site for  $\text{MgAl}_2\text{O}_4\text{:Mn}$  synthesized by solid state reaction at 1400-1600 °C for 5 h). All the samples were single spinel phase as indicated by XRD (shown in Figure 2 and Figure S1). Several diffraction halos with quite low intensity were observed for the precursor heated at 450 °C. Then, crystalline  $\text{MgAl}_2\text{O}_4$  was formed when heated at 700 °C. Intensities of the diffraction peaks got increased and the peak becomes shaper along with the temperature rise. All the diffraction peaks coincide with the reference ( $\text{MgAl}_2\text{O}_4$ , JCPDS No. 47-0254).

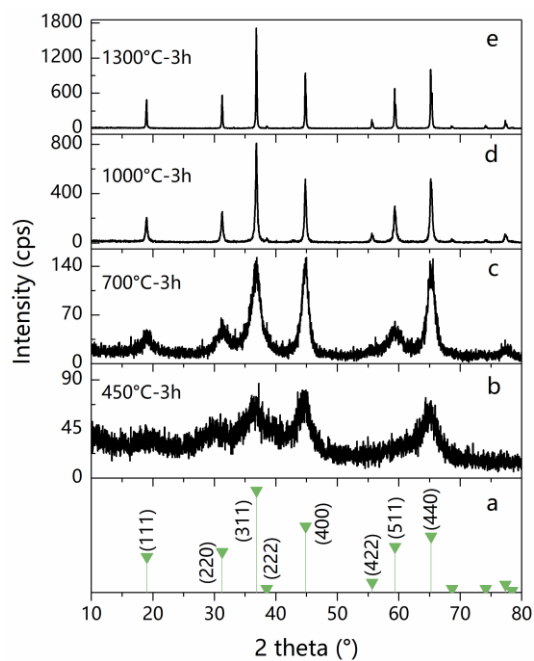
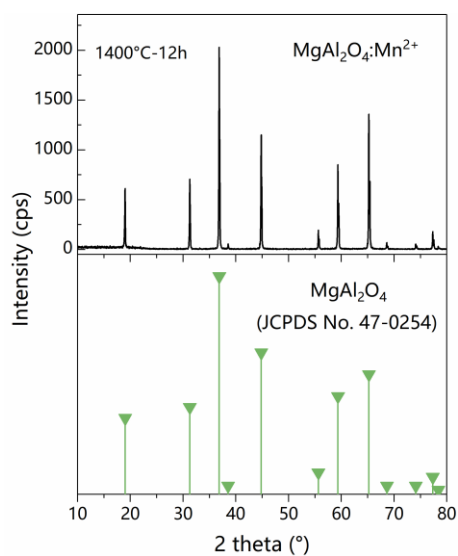


**Figure 2** XRD patterns of the phosphors calcined at 450 °C (b), 700 °C (c), 1000 °C (d), and 1300 °C (e) for 3 h. The standard pattern for  $\text{MgAl}_2\text{O}_4$  (JCPDS card no. 47-0254) was provided as reference (a).



**Supplemental Figure S1** XRD pattern of the spinel phosphor calcined at 1400 °C for 12 h. The standard pattern for  $\text{MgAl}_2\text{O}_4$  (JCPDS card no. 47-0254) was provided as reference.

### 3.2 Temperature-induced inhomogeneous broadening of the luminescence spectra in $\text{MgAl}_2\text{O}_4:\text{Mn}^{4+}$

Figure 3 shows the PLE/PLs of the  $\text{MgAl}_2\text{O}_4:\text{Mn}^{4+}$  phosphors prepared at 700-1300 °C (PL/PLE of the phosphor synthesized at 1400 °C showing  $\text{Mn}^{2+}$  green emission was provided in supplemental Figure S2). The PLEs consist of two broad bands in the 250-350 nm and 400-500 nm range, originating from the  $\text{O}^{2-} \rightarrow \text{Mn}^{4+}$  charge transfer (CT) transition and the spin-allowed  ${}^4\text{A}_{2g} \rightarrow {}^4\text{T}_{1g}$  and  ${}^4\text{A}_{2g} \rightarrow {}^4\text{T}_{2g}$  transitions. The PLE bands in the blue spectral range is peaking at 440 nm, suitable for blue LED pumping. The emissions are peaking at 651 nm caused by the ZPL emission and/or the associated phonon sidebands, and show no clear fine structure. The PLs exhibit a single asymmetric broad band, with intensity decreasing more steeply with increasing photon energy. Although the PLs are quite broad which is similar with a case of spin-allowed transition, we believe that the emitting level is  ${}^2\text{E}_g$  instead of  ${}^4\text{T}_{2g}$  since  $\text{Mn}^{4+}$  tends to experience a strong crystal field due to a high positive charge than  $\text{Cr}^{3+}$ .

Moreover, by comparing the PLs measured at temperature of 100 K and 293 K, the ZPL emission can be verified to be at 651 nm ( $15\,361\text{ cm}^{-1}$ ) as the anti-Stokes emission (higher energy side of ZPL emission) got enhanced at 293 K than that measured at 100 K. This thus demonstrated a quite high  ${}^2\text{E}_g \rightarrow {}^4\text{A}_{2g}$  transition energy of  $\text{Mn}^{4+}$  among the so-far reported oxide hosts;<sup>34</sup> higher  ${}^2\text{E}_g \rightarrow {}^4\text{A}_{2g}$  transition energy is only achieved in some germanates (such as  $\text{Mg}_4\text{GeO}_6$ ,  $\text{Mg}_{14}\text{Ge}_5\text{O}_{24}$ ) and arsenates (such as  $\text{Mg}_6\text{As}_2\text{O}_{11}$ ). Such high ZPL energy demonstrates the advantage of developing this spinel phosphor.

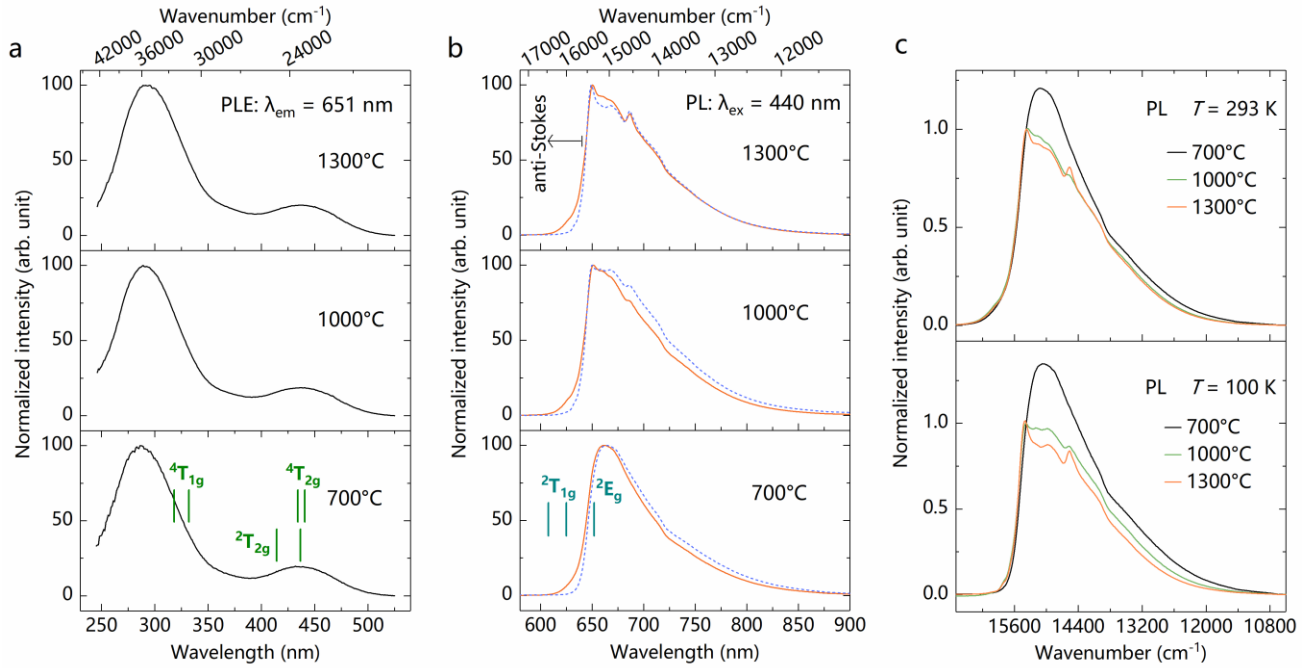
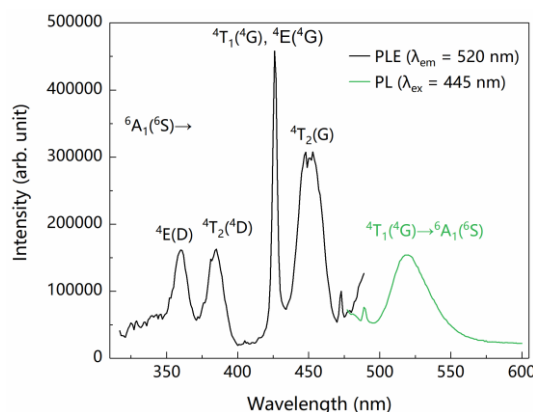


**Figure 3** Normalized PLE (a) and PL (b) of the  $\text{MgAl}_2\text{O}_4:\text{Mn}^{4+}$  phosphors heated at 700 °C, 1000 °C, or 1300 °C for 3 h, respectively. The PLs were comparatively measured at  $T = 293$  K (red) and 100 K (blue) in (b). (c) PLs of the  $\text{MgAl}_2\text{O}_4:\text{Mn}^{4+}$  phosphors normalized at the ZPL emission intensity at 651 nm ( $15\,361\text{ cm}^{-1}$ ).

The  $\text{Mn}^{4+}$  energy levels in  $\text{MgAl}_2\text{O}_4$  were also calculated. A large cluster consisting of 62210 ions was build up to ensure the proper convergence of the crystal lattice sums needed for calculations of the crystal field parameters. The trigonal symmetry of the Al site was confirmed by the structure of the crystal field Hamiltonian, in which only the following crystal field parameters were not zero (in  $\text{cm}^{-1}$ , Stevens normalization):  $B_2^0 = 2488$ ,  $B_4^0 = -4428$ ,  $B_4^3 = 107938$ . The Racah parameters values were (in  $\text{cm}^{-1}$ )  $B = 800$  and  $C = 3157$ , respectively. The calculated  $\text{Mn}^{4+}$  energy levels (in  $\text{cm}^{-1}$ ; only those energy levels which are relevant for the discussion of the spectroscopic measurements are given; the asterisk indicates the orbital doublet states) are as follows:  ${}^4\text{A}_{2g} - 0$ ;  ${}^2\text{E}_g - 15361^*$ ;  ${}^2\text{T}_{1g} - 16025^*$  and  $16483$ ;  ${}^2\text{T}_{2g} - 22924$  and  $24121^*$ ;  ${}^4\text{T}_{2g} - 22718^*$  and  $23058$ ;  ${}^4\text{T}_{1g} - 30133$  and  $31526^*$ . The character of the orbital triplets splitting into a singlet and a doublet states is also in line with the trigonal symmetry of the  $\text{Mn}^{4+}$  position. Agreement with the experimental spectra is visualized in [Figure 3](#), where the calculated energy levels are shown by the vertical bars.

The PLs of the phosphors heated at 1000 and 1300 °C with higher crystallinity are consistently

peaking at 651 nm. However, there exists obvious difference between these PLs in the lower energy sides (the phonon sidebands), which thus induced varying FWHM (Full-Width at Half-Maximum) of the PLs. The FWHM can be evaluated in two ways, either the value difference at the half-maximum, or the value of the integrated area dividing the peak. Considering the asymmetric feature of the PLs, we here evaluate the FWHMs using the second method. Figure 3c shows the PLs which were normalized at the 651 nm ZPL emission. The estimated FWHMs using such normalized PLs are  $2093\text{ cm}^{-1}$  ( $T = 293\text{ K}$ )/ $2416\text{ cm}^{-1}$  ( $T = 100\text{ K}$ ),  $1811\text{ cm}^{-1}$  ( $T = 293\text{ K}$ )/ $1936\text{ cm}^{-1}$  ( $T = 100\text{ K}$ ), and  $1772\text{ cm}^{-1}$  ( $T = 293\text{ K}$ )/ $1733\text{ cm}^{-1}$  ( $T = 100\text{ K}$ ), for the phosphors synthesized at  $700\text{ }^{\circ}\text{C}$ ,  $1000\text{ }^{\circ}\text{C}$ , and  $1300\text{ }^{\circ}\text{C}$ , respectively. Although the FWHM values change with the way of normalization, we found the trend that the increase in the heating temperature of the spinel phosphors leads to a decrease in the FWHM of the PLs. Such FWHM variation is not so significant, but reflects some interesting intrinsic change of factors affecting the  $\text{Mn}^{4+} {}^2\text{E}_g \rightarrow {}^4\text{A}_{2g}$  transition.



**Supplemental Figure S2** Photoluminescence spectra of the  $\text{MgAl}_2\text{O}_4:\text{Mn}^{2+}$  phosphor calcined at  $1400\text{ }^{\circ}\text{C}$  for 12 h. The corresponding energy transitions were assigned based on Ref. [1]. Ref. [1]: E. H. Song, Y. Y. Zhou, Y. Wei, X. X. Han, Z. R. Tao, R. L. Qiu, Z. G. Xia and Q. Y. Zhang. A thermally stable narrow-band green-emitting phosphor  $\text{MgAl}_2\text{O}_4:\text{Mn}^{2+}$  for wide color gamut backlight display application. *J. Mater. Chem. C*, 2019, 7, 8192-8198.

Generally, the origin for the broad FWHM of the PL bands can be the inhomogeneous broadening effect, which is a well-known phenomenon observed in solid solution phosphors exhibiting  $d-f$  parity-allowed transition, for example, the  $\text{Lu}_3(\text{Al}_{2-x}\text{Mg}_x)(\text{Al}_{3-x}\text{Si}_x)\text{O}_{12}:\text{Ce}^{3+}$  ( $x = 0.5-2.0$ )<sup>35</sup>, the  $\text{Y}_x\text{Lu}_{3-x}\text{MgAl}_3\text{SiO}_{12}:\text{Ce}^{3+}$  ( $x = 0-3$ )<sup>36</sup> and the  $M_3(\text{PO}_4)_2:\text{Eu}^{2+}$  ( $M = \text{Ca}, \text{Sr}, \text{Ba}$ )<sup>37</sup> phosphors. The

inhomogeneous broadening of the PL bands is induced by a higher diversity of local coordination environments of the activator ions in solid-solution phases. We presume that the FWHM deviation of PLs for  $\text{MgAl}_2\text{O}_4:\text{Mn}^{4+}$  exhibiting the  $d-d$  parity-forbidden transition can be explained in the same way. The diversity of the local coordination environments can be induced by multiple ways,<sup>38</sup> for instance, the cation interstitial, the cation/anion vacancy, and the cation antisite-occupation, which finally lead to the first nearest coordination sphere (*i.e.*, the  $\text{MnO}_6$  octahedrons) offsetting an average situation. Among them, the cation anti-site occupation ( $\text{Mg}_{\text{Mg}}^x + \text{Al}_{\text{Al}}^x \rightarrow \text{Al}_{\text{Mg}}^x + \text{Mg}_{\text{Al}}^x$  in Kröger-Vink notation) is known to occur in synthetic spinel. As the concentration of such  $\text{Mg} \leftrightarrow \text{Al}$  anti-site disorder is influenced by the thermal history, it may be one origin for the observed inhomogeneous broadening. This anti-site disorder infers self-compensation of  $\text{Mn}_{\text{Al}}$ -substitution with  $\text{Mg}^{2+}$ . Because of the antisite associated charge compensation, there is a range of distortion around  $\text{Mn}^{4+}$  ions, which tends to obscure the fine-structure details of the zero-phonon  ${}^2\text{E}_g \rightarrow {}^4\text{A}_{2g}$  transitions of  $\text{Mn}^{4+}$  spectrum.<sup>8</sup> Meanwhile, the anti-site disorder may contribute to an increase in phonon scattering, which causes the FWHM broadening of PLs.

We thus try to evaluate semi-quantitatively the anti-site disorder concentrations by checking the lattice dimension evolution *via* Rietveld refinement. Theoretically, if we replace  $\text{Mg}^{2+}$  in tetrahedron  $8a$  site by  $x$  amount of  $\text{Al}^{3+}$ , the average ion radii of the  $8a$  site ( $\text{IR}_{8a}$ ) becomes to be  $x*0.39 + (1-x)*0.57$  ( $r_{\text{Al}^{3+}, \text{CN}=4} = 0.39 \text{ \AA}$ ;  $r_{\text{Mg}^{2+}, \text{CN}=4} = 0.57 \text{ \AA}$ ) (CN: coordination number). Since the octahedron  $16d$  site has twice bigger multiplicity than that of the  $8a$  site, the  $16d$  site loses only  $x/2$   $\text{Al}^{3+}$ . Thus, the average ion radii of the  $16d$  site ( $\text{IR}_{16d}$ ) becomes to be  $(1-x/2)*0.535 + (x/2)*0.72$  ( $r_{\text{Mg}^{2+}, \text{CN}=6} = 0.72 \text{ \AA}$ ,  $r_{\text{Al}^{3+}, \text{CN}=6} = 0.535 \text{ \AA}$ ). The variation of lattice parameter with respect to anti-site disorder in  $(\text{Mg}_{1-i}\text{Al}_i)[\text{Mg}_i\text{Al}_{2-i}]\text{O}_4$  has been shown to be small; a change of 0.1 in  $i$  modifies the lattice parameter by just  $0.0025 \text{ \AA}$ .<sup>39</sup> Thus, the cell volume ( $V$ ) change is chosen to reveal the anti-site disorder.  $V$  should be proportional to  $1/3(\text{IR}_{8a}) + 2/3(\text{IR}_{16d})$  for this cubic phase, *i.e.*,  $1/3V \propto 1.64 + 0.005x$ . Thus, migration of  $x/2$   $\text{Al}^{3+}$  from the  $16d$  site to  $x$  amount  $\text{Al}^{3+}$  in the  $8a$  site leads to small increase in  $V$ . Rietveld refinement was performed (occupancy of Al/Mg were not refined because of too small difference of their X-ray atomic scattering power), as provided in [Figure 4a-c](#). The  $V$  behavior per  $T$  was plotted in [Figure 4d](#). The refinements were stable and ended with

relatively low  $R$ -factors (Table 2). Coordinates of atoms and main bond lengths are listed in Table 3 and Table 4, respectively. Although the  $V$  for the sample sintered at 700 °C has relatively large esd (effective standard deviation), it is clear that  $V$  increases with the calcination temperature, and thus, the concentration of anti-site disorder increases in the order of  $T = 700, 1000, 1300$  °C. Such  $V$ - $T$  trend is in accordance with what has been observed by the *in-situ* measurement on  $\text{MgAl}_2\text{O}_4$  single crystal<sup>40</sup>.

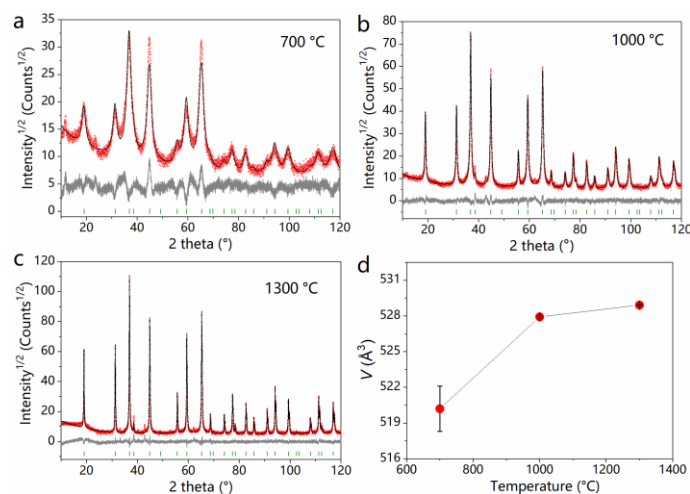


**Figure 4** Observed (red), calculated (black), and difference (gray) XRD profiles for the  $\text{MgAl}_2\text{O}_4:\text{Mn}^{4+}$  phosphors synthesized at temperature of (a) 700 °C, (b) 1000 °C, and (c) 1300 °C refined by Rietveld method. Bragg reflections are indicated with green ticks. (d) Cell volume behavior per  $T$ .

**Table 2** Main parameters of processing and refinement of  $\text{MgAl}_2\text{O}_4:\text{Mn}^{4+}$

$T$ , °C	Space Group	Cell parameters (Å), Cell Volume (Å <sup>3</sup> )	$R_{\text{wp}}$ , $R_{\text{p}}$ , $R_{\text{Brag}}$ , $\chi^2$
700	$Fd-3m$	$a = 8.0712$ (12), $V = 525.80$ (22)	14.08, 11.59, 5.26, 1.83
1000	$Fd-3m$	$a = 8.0853$ (5), $V = 528.55$ (10)	10.92, 8.10, 2.01, 1.36
1300	$Fd-3m$	$a = 8.08630$ (7), $V = 528.748$ (14)	12.15, 8.33, 1.62, 1.52

**Table 3** Fractional atomic coordinates and isotropic displacement parameters ( $\text{\AA}^2$ ) of  $\text{MgAl}_2\text{O}_4:\text{Mn}^{4+}$ 

Atom	$x$	$y$	$z$	$B_{\text{iso}}$	Occupation
$T = 700\text{ }^\circ\text{C}$					
Mg	0.125	0.125	0.125	1.0 (7)	1
Al	0.5	0.5	0.5	1.0 (4)	1
O	0.2556 (5)	0.2556 (5)	0.2556 (5)	0.8 (6)	1
$T = 1000\text{ }^\circ\text{C}$					
Mg	0.125	0.125	0.125	0.54 (17)	1
Al	0.5	0.5	0.5	0.66 (9)	1
O	0.26072 (15)	0.26072 (15)	0.26072 (15)	0.76 (13)	1
$T = 1300\text{ }^\circ\text{C}$					
Mg	0.125	0.125	0.125	0.31 (6)	1
Al	0.5	0.5	0.5	0.47 (6)	1
O	0.26177 (12)	0.26177 (12)	0.26177 (12)	0.55 (7)	1

**Table 4** Main bond lengths ( $\text{\AA}$ ) of  $\text{MgAl}_2\text{O}_4:\text{Mn}^{4+}$ 

$T = 700\text{ }^\circ\text{C}$			
Mg—O	1.826 (4)	Al—O <sup>i</sup>	1.974 (4)
$T = 1000\text{ }^\circ\text{C}$			
Mg—O	1.9006 (12)	Al—O <sup>i</sup>	1.9385 (12)
$T = 1300\text{ }^\circ\text{C}$			
Mg—O	1.9156 (10)	Al—O <sup>i</sup>	1.9311 (10)

Symmetry codes: (i)  $-x+1, z+1/4, y+1/4$ 

The fact that the anti-site disorder increases with temperature rise in the  $\text{MgAl}_2\text{O}_4:\text{Mn}^{4+}$  phosphors is contradictory to the observation that the FWHM decreases with temperature rise, since higher disorder degree of local coordination generally leads to larger FWHM of an electric dipole transition. Therefore, we further presume that there exists another factor which plays a more important role than the anti-site disorder that is affecting the FWHM of the  $\text{MgAl}_2\text{O}_4:\text{Mn}^{4+}$  luminescence. It is noticed from [Table 3](#) that at higher temperatures, the isotropic displacement parameter ( $B_{\text{iso}}$ ) of all constituent atoms exhibits clear decrease. In spinel, the oxygen atoms locate at the  $(u,u,u)$  site; since

Mn<sup>4+</sup> dopants are bonded with oxygen, the thermal effect on the  $B_{\text{iso}}$  parameter of the  $(u,u,u)$  site can account for the FWHM variation. The Stokes vibronic emissions of Mn<sup>4+</sup>  ${}^2E_g \rightarrow {}^4A_{2g}$  forbidden transition gain intensity from the *ungerade* vibrational modes including the asymmetric bending ( $\nu_6$ ,  $\nu_4$ ) and asymmetric stretching ( $\nu_3$ ) of the MnO<sub>6</sub> moieties. To verify the correlation between the decrease of the  $B_{\text{iso}}$  parameter and the vibrational modes of the spinel lattice, we collected the Raman spectra in the spectral range 200-900 cm<sup>-1</sup>, as shown in Figure 5. Three relatively clear Raman modes are observed and marked accordingly<sup>41</sup>. When heated at 700 °C, the halo Raman modes with very weak intensity is seen, and it is difficult to identify the modes. When heat at 1000 °C, the  $E_g$  Raman mode is noticeable, which becomes narrower in the sample heated at 1300 °C. Comparison of the Raman spectra collected for these three phosphors indicates that the structural rigidness gradually increased with the heating temperature. Thus, the decrease of  $B_{\text{iso}}$  parameter of oxygen atoms (of course, also the Al and Mg atoms) was verified by Raman measurement, besides of the evidence from the Rietveld refinement on the XRD patterns. Such decrease of  $B_{\text{iso}}$  parameter of consistent atoms leads to the restrain of the strength of phonon scattering and the strength of electron-phonon coupling, as well as the ordering of the *ungerade* vibrational modes ( $\nu_6$ ,  $\nu_4$ ,  $\nu_3$ ), which result in the decrease of observed PL FWHM of Mn<sup>4+</sup>  ${}^2E_g \rightarrow {}^4A_{2g}$  transition in MgAl<sub>2</sub>O<sub>4</sub>. Wang *et al.*<sup>42</sup> prepared MgAl<sub>2</sub>O<sub>4</sub>:Eu<sup>3+</sup> by a solution combustion method with heating temperatures of 700-1200 °C, and they demonstrate that the Debye temperature of samples show positive relationship with the calcination temperature. Thus, the decrease of  $B_{\text{iso}}$  parameter of all atoms in the present MgAl<sub>2</sub>O<sub>4</sub>:Mn<sup>4+</sup> phosphors can be also regarded as the dynamic improvement of structural rigidness.

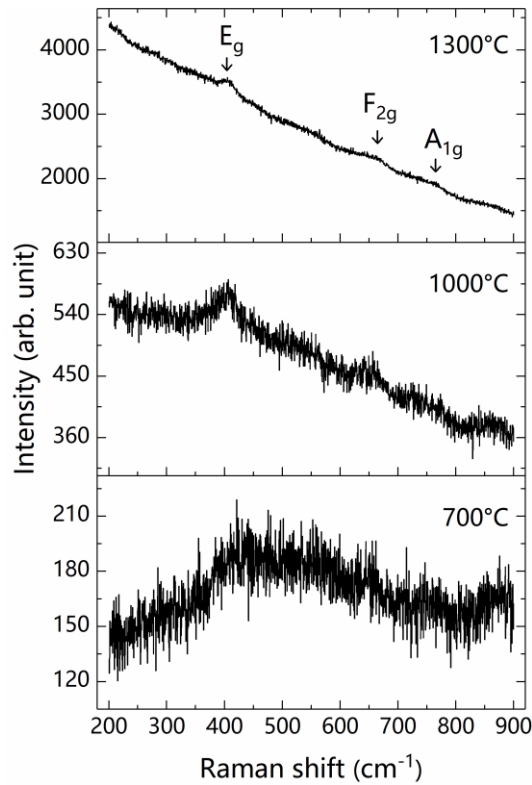


**Figure 5** Raman spectra of the  $\text{MgAl}_2\text{O}_4:\text{Mn}^{4+}$  phosphors synthesized at temperature of 700 °C, 1000 °C, and 1300 °C. The observed Raman modes are marked.

### 3.3 Chemically induced order-disorder in $\text{MgAl}_2\text{O}_4:\text{Mn}^{4+}$ phosphor and the luminescence property

Although the inhomogeneous broadening of the luminescence spectra in  $\text{MgAl}_2\text{O}_4:\text{Mn}^{4+}$  is mainly induced by the decrease of  $B_{\text{iso}}$  parameter of consistent atoms, the effect of the Mg-Al anti-site disorder cannot be fully neglected. As a proof of concept, we here prepare the  $\text{MgAl}_2\text{O}_4:\text{Mn}^{4+}$  at really high temperature (1550 °C for 6 h), but introduce  $\text{Ga}^{3+}$  with larger ionic size to partially replace  $\text{Al}^{3+}$  as a way to control the degree of Mg-Al antisite disorder.

The  $\text{MgAl}_2\text{O}_4$  is the parent compound of the spinel group, the compositions of which can be generalized as  $\text{AB}_2\text{X}_4$ . In a fully inverse spinel, 1/8 of the tetrahedral sites are filled with  $\text{B}^{3+}$  and 1/4 of the octahedral sites are filled with  $\text{A}^{2+}$  and 1/4 are filled with  $\text{B}^{3+}$  in a fully inverse spinel.<sup>43</sup> The relative distributions of the cations at these octahedral/tetrahedral sites are influenced by the ionic radius and electronegativity of the cations.<sup>44</sup> Thus, besides of temperature, the antisite disorder can be induced chemically. For example, the spinel of  $\text{MgGa}_2\text{O}_4$  has larger degree of site inversion than  $\text{MgAl}_2\text{O}_4$  due to the larger ionic size of  $\text{Ga}^{3+}$  than  $\text{Al}^{3+}$  (unit cells shown in Figure 6a, b). Moreover,

it has been demonstrated that complete solid solution can form between  $\text{MgAl}_2\text{O}_4$  and  $\text{MgGa}_2\text{O}_4$  at  $1550\text{ }^\circ\text{C}$ .<sup>45</sup> We thus came up with the idea to prepare  $\text{MgAl}_{2-x}\text{Ga}_x\text{O}_4:\text{Mn}^{4+}$  solid solution phosphors to observe the FWHM evolution of the PLs in response to the progressive anti-site disordering induced by the substitution of  $\text{Al}^{3+}$  by  $\text{Ga}^{3+}$ . XRD confirmed the formation of single phase when  $x$  is equal to 0, 0.5 and 1.0 by comparing the measured pattern with these of  $\text{MgAl}_2\text{O}_4$  (JCPDS No. 047-254) and  $\text{MgAl}_{1.04}\text{Ga}_{0.96}\text{O}_4$  (JCPDS No. 04-007-2715) (as shown in Figure 6c). Seen from Figure 6e, the ZPL of  $\text{Mn}^{4+} {}^2\text{E}_g \rightarrow {}^4\text{A}_{2g}$  transition is almost independent on crystal field strength but varies with the different nephelauxetic effect experienced by the  $\text{Mn}^{4+}$  3d orbital. Thus, the PLs ( $\lambda_{\text{ex}} = 440\text{ nm}$ ) of the  $\text{MgAl}_{2-x}\text{Ga}_x\text{O}_4:\text{Mn}^{4+}$  phosphors were normalized at the respective peak emissions. Indeed, seen from Figure 6d, the PL is becoming broadening with the intensity of the longer-wavelength emission getting enhanced as  $x$  changes from 0 to 1.0. Thus, using the chemically induced order-disorder in  $\text{MgAl}_2\text{O}_4:\text{Mn}^{4+}$ , the relationship between the large FWHM and the anti-site defect can be further verified. Since the preparation was conducted at quite high temperature of  $1550\text{ }^\circ\text{C}$ , the Raman modes are clear (see the Raman spectrum measured for the  $x = 0$  sample in Figure 6f) but relatively broad indicating the existence of anti-site disorder in the synthetic spinel. With the introduction of  $\text{Ga}^{3+}$ , the  $F_{2g}$  and  $A_{1g}$  Raman modes get their intensity enhanced associated with small shift, suggesting the cooperation of  $\text{Ga}^{3+}$  into the lattice and more importantly, the change of the dominating vibrational modes. Although the  $\text{Mn}^{4+} {}^2\text{E}_g \rightarrow {}^4\text{A}_{2g}$  transition mainly couples with the  $\nu_6$  vibrational modes to gain intensity, the change of dominating vibrational modes would reasonably change the relative intensity of the phonon sideband emissions. Thus, a varying FWHM of PLs depending on the  $\text{Al}^{3+}$ - $\text{Ga}^{3+}$  substitution is observed by this chemically induced anti-site disorder.

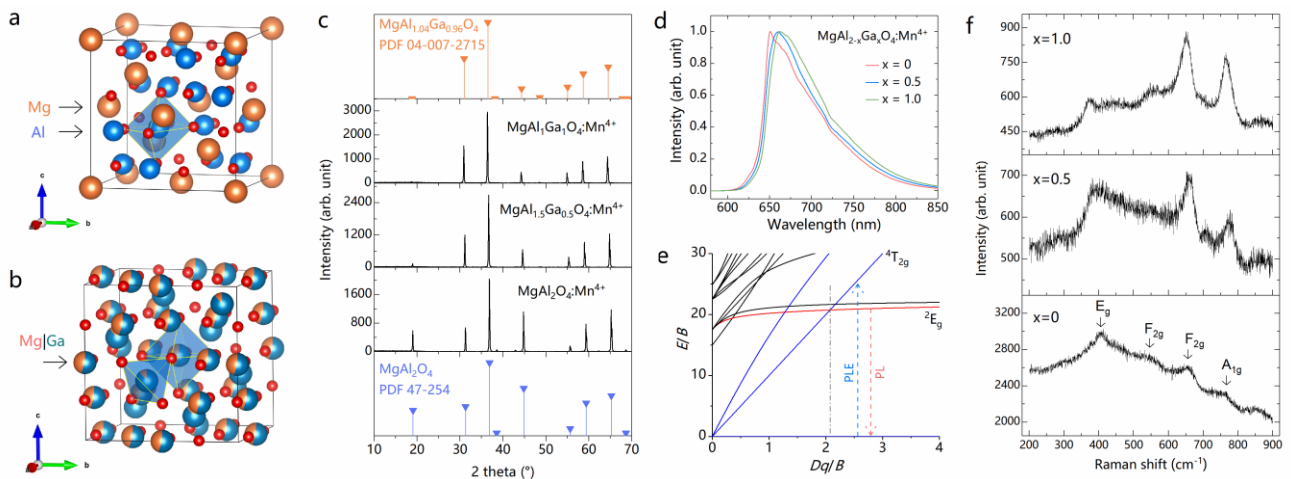


**Figure 6** (a) Unit cells of  $\text{MgAl}_2\text{O}_4$  (ICSD\_CollCode31373) and (b) unit cell of  $\text{MgGa}_2\text{O}_4$  (ICSD\_CollCode4806). Drawn with VESTA<sup>46</sup>. (c) XRD patterns and (d) PL spectra ( $\lambda_{\text{ex}} = 440$  nm) of the  $\text{MgAl}_{2-x}\text{Ga}_x\text{O}_4:\text{Mn}^{4+}$  phosphors. (e) Tanabe-Sugano diagram for a  $d^3$  ion. (f) Raman spectra of the  $\text{MgAl}_{2-x}\text{Ga}_x\text{O}_4:\text{Mn}^{4+}$  ( $x = 0, 0.5, 1.0$ ) phosphors.

### 3.4 Abnormal luminescence thermal quenching behavior of $\text{MgAl}_2\text{O}_4:\text{Mn}^{4+}$

The PL thermal quenching of the spinel phosphors were studied in the range of 100–470 K under excitation of 440 nm laser diode, as shown in Figure 7. The quenching temperature ( $T_{50\%}$ , the temperature at which the intensity drops to be half of the initial value) are 250 K, 352 K, and 400 K for the phosphors heated at 700 °C, 1000 °C, and 1300 °C, respectively, which shows significant change with calcination temperature. Although the  $T_{50\%}$  may be overestimated since the PL steadily may decrease with temperature rise between 0 K and 100 K, it is clear that the  $T_{50\%}$  of  $\text{Mn}^{4+}$  luminescence of the spinel phosphors shows dependence on the calcination temperature of the samples: high calcination temperature leads to high  $T_{50\%}$  of the sample.

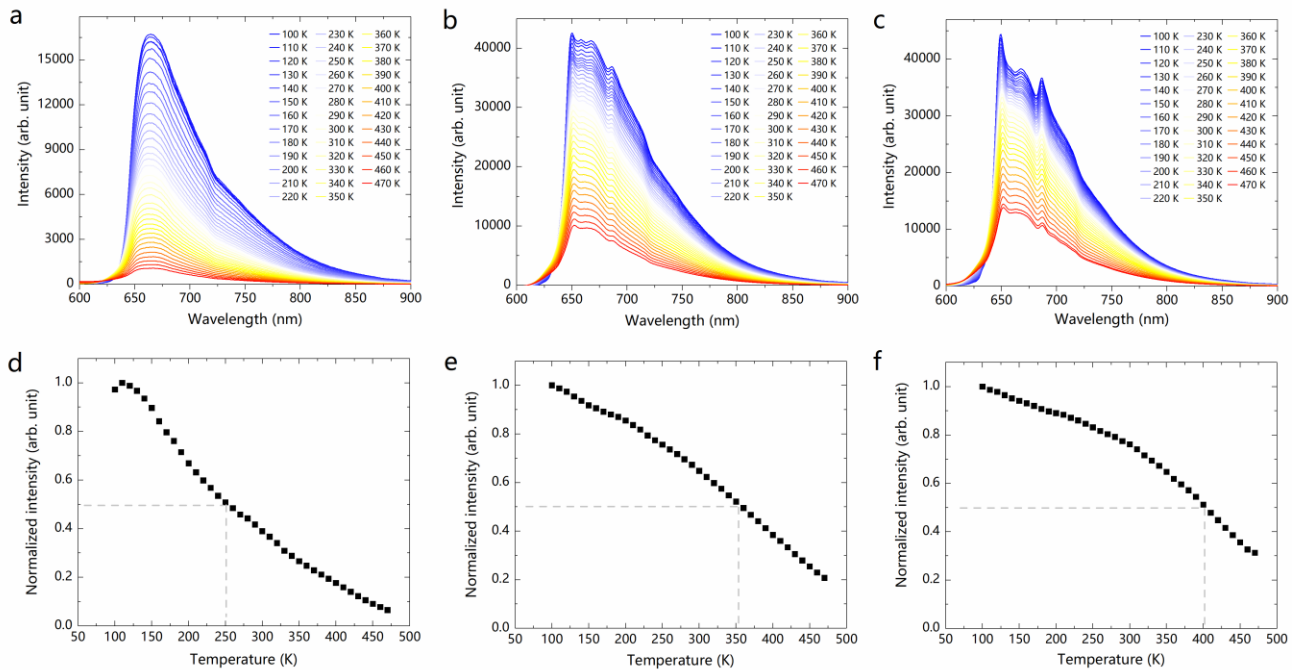


**Figure 7** Photoluminescence thermal quenching of the  $\text{MgAl}_2\text{O}_4:\text{Mn}^{4+}$  phosphors prepared at temperature of (a) 700 °C, (b) 1000 °C, (c) 1300 °C ( $\lambda_{\text{ex}} = 440$  nm). The evolution of the integrated PL intensity (in the spectral range from 600 nm to 900 nm) against temperature were shown in (d),

(e), (f), respectively.

In the paper by Senden et al.<sup>47</sup> and by our previous work<sup>48</sup>, we have demonstrated a consistence between the  ${}^4T_{2g}$  level and the  $T_{50\%}$ . However, from the present observation, it is seen that even with the same  ${}^4T_{2g}$  level of  $Mn^{4+}$  in  $MgAl_2O_4$  spinel, the  $T_{50\%}$  can differ significantly from 250 K, 352 K, and to be 400 K. That is to say, the  $T_{50\%}$  practically also depends on the preparation history; key factors associated with the preparation history may include the crystallinity and anti-site disorder concentration. In order to explore the intrinsic thermal quenching temperature of  $Mn^{4+}$  luminescence in  $MgAl_2O_4$ , we thus try to prepare the  $MgAl_2O_4:Mn^{4+}$  phosphor with high crystallinity. A molten salt method which provides an unstrained environment for crystal growth was employed<sup>49</sup>. The product is highly crystalline spinel with noticeable distinguished tetragonal-bipyramids morphology (shown in Figure 8d). Large portion of spinel particles are seen to exhibit the well-developed crystalline planes, indicating the growth in an approximate-equilibrium condition. Such morphology quite differs from these observed for the samples prepared by the co-precipitation method (Figure 8a-c) which are large particles with ununiform size of 1-20  $\mu m$ . The large particle size of  $MgAl_2O_4:Mn^{4+}$  phosphors prepared by the co-precipitation method is due to the formation of  $AlOOH$  (which is very glutinous favorable for particle aggregation) in the precursor as well as a long period of aging.

The thermal quenching behavior (Figure 9ab) of the  $MgAl_2O_4:Mn^{4+}$  phosphor prepared by the molten salt method shows high similarity with that of the phosphor prepared by co-precipitation and heated at 1300 °C. The  $T_{50\%}$  estimated by this sample is around 390 K (Figure 9c), which is very close to the value estimated in Figure 7f; thus, the intrinsic  $T_{50\%}$  for  $Mn^{4+}$  luminescence in  $MgAl_2O_4$  is believed to be around 390 K-400 K. Currently, the widely proposed thermal quenching mechanisms for  $Mn^{4+}$  luminescence is thermal assisted crossover from the emitting  ${}^2E_g$  state to the Franck-Condon shifted  ${}^4T_{2g}$  level and then non-radiative relaxation to the  ${}^4A_{2g}$  level. According to the configuration coordinate model (Figure 9d), if the  ${}^4T_{2g}$  potential curve is right-shifted ( ${}^4T_{2g}^*$ ) further offsetting the  ${}^4A_{2g}$  level, the activation energy  $E_a$  for thermal crossover quenching decreases to be a smaller  $E_a^*$ . Thus, the observed  $T_{50\%}$  dependence on the calcination temperature can be regarded as the left-shift of the  ${}^4T_{2g}$  potential curve with lower electron-phonon coupling at higher calcination temperature of the co-precipitated sample.

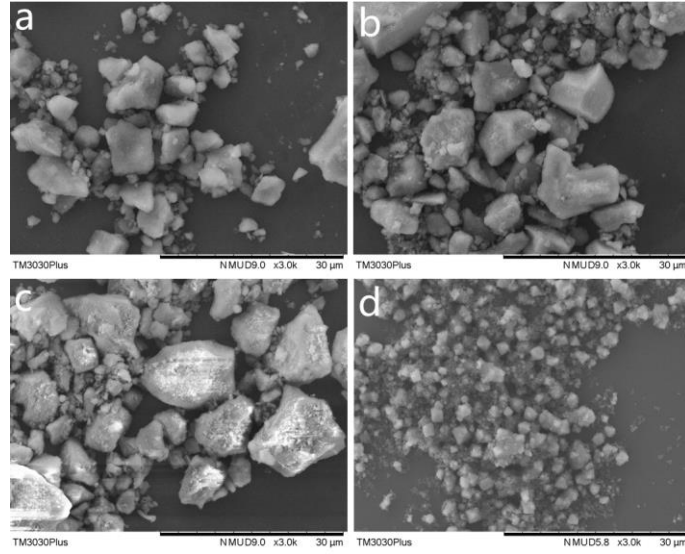


**Figure 8** SEM images of  $\text{MgAl}_2\text{O}_4:\text{Mn}^{4+}$  phosphors prepared by the co-precipitation method and heated at: (a) 700 °C, (b) 1000 °C, and (c) 1300 °C. (d) shows the SEM images of  $\text{MgAl}_2\text{O}_4:\text{Mn}^{4+}$  phosphor prepared by the molten salt method.

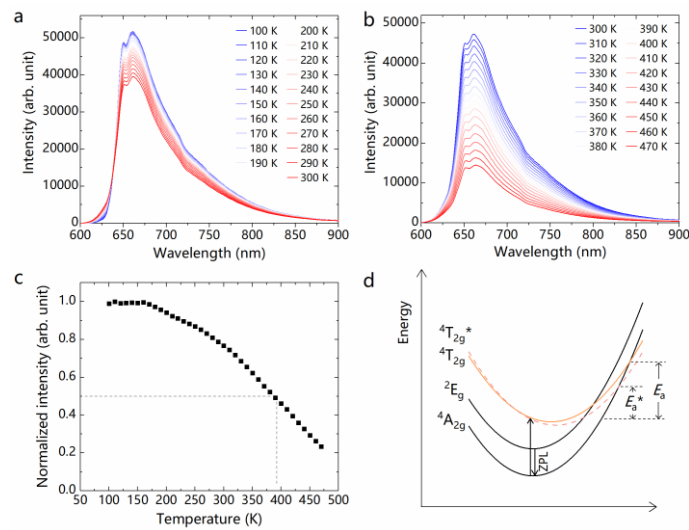


**Figure 9** Photoluminescence thermal quenching of the  $\text{MgAl}_2\text{O}_4:\text{Mn}^{4+}$  phosphor prepared by the molten salt synthesis: (a) from 100 K to 300 K, (b) from 300 K to 470 K. The evolution of the integrated PL intensity (in the spectral range from 600 nm to 900 nm) against temperature were shown in (c). (d) The thermal assisted crossover model explaining the thermal quenching of  $\text{Mn}^{4+}$  luminescence and the  $T_{50\%}$  dependence on the calcination temperature.

## 4 Conclusions

We prepared the  $\text{MgAl}_2\text{O}_4:\text{Mn}^{4+}$  red-emitting phosphor for blue LED pumped white lighting using the co-precipitation method sintered at different temperatures (700-1300 °C). The phosphors exhibit ultrabroadband emission peaking at 651 nm. The synthetic spinel structure accommodates  $\text{Mg}^{2+} \leftrightarrow \text{Al}^{3+}$  anti-site disorder, which leads to the ultrabroadband emission without fine structure between ZPL and phonon sideband emissions. The large FWHM showed dependence both on the calcination temperature as well as the partial substitution of  $\text{Al}^{3+}$  by  $\text{Ga}^{3+}$ . The increase of calcination temperature from 700 °C to 1300 °C leads to a decrease of the anti-site disorder concentration while the substitution of  $\text{Al}^{3+}$  by  $\text{Ga}^{3+}$  chemically leads to an increase of the anti-site disorder concentration. By means of Rietveld refinement and Raman technique, we demonstrate that such variation of the PL FWHM is a sum effect of structural ordering (isotropic displacement decrease of constituent atoms) and the  $\text{Mg} \leftrightarrow \text{Al}$  anti-site disorder. The phosphor heated at higher calcination temperature exhibits a higher thermal quenching temperature  $T_{50\%}$ , which can be explained by the lower electron-phonon coupling in the configuration coordinate model. The intrinsic  $T_{50\%}$  for  $\text{Mn}^{4+}$  luminescence in  $\text{MgAl}_2\text{O}_4$  is believed to be around 390 K-400 K.

## Acknowledgements

This study was supported by the National Natural Science Foundation of China (Grant No. 51902291), the China Postdoctoral Science Foundation (2019M662524) and the Postdoctoral Research Sponsorship in Henan Province (19030025). X.H. also thanks the support from China Postdoctoral Science Foundation (2019M652574). J.U. and S.T. were also supported by the JSPS KAKENHI (16K05934), and M.M. was also supported by the RFBR (19-52-80003).

## References

- 1 Z. Xia and A. Meijerink, *Chem. Soc. Rev.*, 2017, **46**, 275–299.
- 2 H. F. Sijbom, R. Verstraete, J. J. Joos, D. Poelman and P. F. Smet, *Opt. Mater. Express*, 2017, **7**, 3332–3365.
- 3 Z. Zhou, N. Zhou, M. Xia, M. Yokoyama and H. T. (Bert) Hintzen, *J. Mater. Chem. C*, 2016, **4**, 9143–9161.
- 4 E. Langenberg, E. Ferreira-Vila, V. Leborán, A. O. Fumega, V. Pardo and F. Rivadulla, *APL Mater.*, 2016, **4**, 104815.

- 5 Y. Tanabe and S. Sugano, *J. Phys. Soc. Japan*, 1954, **9**, 766–779.
- 6 Y. D. Xu, D. Wang, L. Wang, N. Ding, M. Shi, J. G. Zhong and S. Qi, *J. Alloys Compd.*, 2013, **550**, 226–230.
- 7 M. Peng, X. Yin, P. A. Tanner, C. Liang, P. Li, Q. Zhang and J. Qiu, *J. Am. Ceram. Soc.*, 2013, **96**, 2870–2876.
- 8 J. F. Donegan, T. J. Glynn, G. F. Imbusch and J. P. Remeika, *J. Lumin.*, 1986, **36**, 93–100.
- 9 T. Sasaki, J. Fukushima, Y. Hayashi and H. Takizawa, *J. Lumin.*, 2018, **194**, 446–451.
- 10 T. Jansen, T. Jüstel, M. Kirm, S. Vielhauer, N. M. Khaidukov and V. N. Makhov, *J. Lumin.*, 2018, **198**, 314–319.
- 11 L. Wang, Y. Xu, D. Wang, R. Zhou, N. Ding, M. Shi, Y. Chen, Y. Jiang and Y. Wang, *Phys. status solidi*, 2013, **210**, 1433–1437.
- 12 Y. Xu, L. Wang, B. Qu, D. Li, J. Lu and R. Zhou, *J. Am. Ceram. Soc.*, , DOI:10.1111/jace.16155.
- 13 B. Wang, H. Lin, J. Xu, H. Chen and Y. Wang, *ACS Appl. Mater. Interfaces*, 2014, **6**, 22905–22913.
- 14 M. G. Brik, I. Sildos, M. Berkowski and A. Suchocki, *J. Phys. Condens. Matter*, 2008, **21**, 25404.
- 15 R. Cao, Q. Xiong, W. Luo, D. Wu, X. Fen and X. Yu, *Ceram. Int.*, 2015, **41**, 7191–7196.
- 16 A. M. Srivastava and M. G. Brik, *Opt. Mater. (Amst.)*, 2017, **63**, 207–212.
- 17 J. Park, G. Kim and Y. J. Kim, *Ceram. Int.*, 2013, **39**, S623–S626.
- 18 Q. Sun, S. Wang, B. Devakumar, L. Sun, J. Liang, X. Huang and Y. Wu, *J. Alloys Compd.*, 2019, **785**, 1198–1205.
- 19 R. Cao, M. Peng, E. Song and J. Qiu, *ECS J. Solid State Sci. Technol.*, 2012, **1**, R123–R126.
- 20 A. M. Srivastava and M. G. Brik, *Opt. Mater. (Amst.)*, 2013, **35**, 1544–1548.
- 21 T. Murata, T. Tanoue, M. Iwasaki, K. Morinaga and T. Hase, *J. Lumin.*, 2005, **114**, 207–212.
- 22 B. D. McNicol and G. T. Pott, *J. Lumin.*, 1973, **6**, 320–334.
- 23 R. Cao, K. N. Sharafudeen and J. Qiu, *Spectrochim. Acta Part A Mol. Biomol. Spectrosc.*, 2014, **117**, 402–405.
- 24 W. Lü, W. Lv, Q. Zhao, M. Jiao, B. Shao and H. You, *Inorg. Chem.*, 2014, **53**, 11985–11990.

- 25 B. W. Nuryadin, A. Sawitri, E. C. S. Mahen and A. Y. Nuryantini, *J. Phys. Conf. Ser.*, 2017, **812**, 12020.
- 26 Y. Zhydachevskii, A. Suchocki, A. Pajęczkowska, A. Kłos, A. Szysiak and A. Reszka, *Opt. Mater. (Amst.)*, 2013, **35**, 1664–1668.
- 27 J.-G. Li, T. Ikegami, J.-H. Lee, T. Mori and Y. Yajima, *J. Eur. Ceram. Soc.*, 2001, **21**, 139–148.
- 28 M. F. Zawrah, H. Hamaad and S. Meko, *Ceram. Int.*, 2007, **33**, 969–978.
- 29 H. Ji, J. Xu, K. Asami, J. Ueda, M. G. Brik and S. Tanabe, *J. Am. Ceram. Soc.*, 2019, **102**, 1316–1328.
- 30 B. Z. MALKIN, *Mod. Probl. Condens. Matter Sci.*, 1987, **21**, 13–50.
- 31 N. M. Avram and M. G. Brik, *Optical Properties of 3d-Ions in Crystals: Spectroscopy and Crystal Field Analysis*, 2013.
- 32 M. G. Brik and Y.-Y. Yeung, *J. Phys. Chem. Solids*, 2008, **69**, 2401–2410.
- 33 Y. Wakui, Y. J. Shan, K. Tezuka, H. Imoto and M. Ando, *Mater. Res. Bull.*, 2017, **90**, 51–58.
- 34 S. Adachi, *ECS J. Solid State Sci. Technol.*, 2020, **9**, 016001.
- 35 H. Ji, L. Wang, M. S. Molokeev, N. Hirosaki, R. Xie, Z. Huang, Z. Xia, O. M. ten Kate, L. Liu and V. V. Atuchin, *J. Mater. Chem. C*, 2016, **4**, 6855–6863.
- 36 H. Ji, L. Wang, M. S. Molokeev, N. Hirosaki, Z. Huang, Z. Xia, O. M. ten Kate, L. Liu and R. Xie, *J. Mater. Chem. C*, 2016, **4**, 2359–2366.
- 37 H. Ji, Z. Huang, Z. Xia, M. S. Molokeev, V. V Atuchin, M. Fang and Y. Liu, *J. Phys. Chem. C*, 2015, **119**, 2038–2045.
- 38 H. Ji, Z. Huang, Z. Xia, M. S. Molokeev, V. V Atuchin and S. Huang, *Inorg. Chem.*, 2014, **53**, 11119–11124.
- 39 J. A. Ball, M. Pirzada, R. W. Grimes, M. O. Zacate, D. W. Price and B. P. Uberuaga, *J. Phys. Condens. Matter*, 2005, **17**, 7621–7631.
- 40 T. Yamanaka and Y. Takéuchi, *Zeitschrift für Krist. - Cryst. Mater.*, 1983, 165, 65–78.
- 41 V. D’Ippolito, G. B. Andreozzi, D. Bersani and P. P. Lottici, *J. Raman Spectrosc.*, 2015, **46**, 1255–1264.
- 42 Z. Wang, S. Jiao, Y. Xu, Q. Zhang, Y. Chen, G. Pang and S. Feng, *J. Lumin.*, 2019, **211**, 108–113.

- 43 K. E. Sickafus, J. M. Wills and N. W. Grimes, *J. Am. Ceram. Soc.*, 1999, **82**, 3279–3292.
- 44 C. Jagadeeshwaran, K. Madhan and R. Murugaraj, *J. Mater. Sci. Mater. Electron.*, 2018, **29**, 18923–18934.
- 45 R. Stalder and K.-H. Nitsch, *J. Am. Ceram. Soc.*, 1997, **80**, 258–260.
- 46 K. Momma and F. Izumi, *J. Appl. Crystallogr.*, 2011, **44**, 1272–1276.
- 47 T. Senden, R. J. A. van Dijk-Moes and A. Meijerink, *Light Sci. Appl.*, 2018, **7**, 8.
- 48 H. Ji, J. Ueda, M. Brik, M. H. Du, D. Chen and S. Tanabe, *Phys. Chem. Chem. Phys.*, 2019, **21**, 25108–25117.
- 49 MgO (A.R., Sinopharm) and Al<sub>2</sub>O<sub>3</sub> (99.99%,  $\gamma$ -phase,  $\leq 20$  nm, Aladdin) were used as raw chemicals. MnCO<sub>3</sub> (A.R., Sinopharm) and LiCl·H<sub>2</sub>O were used as the dopant source and the molten salt. MgO, Al<sub>2</sub>O<sub>3</sub>, and MnCO<sub>3</sub> were weighed according to the formula of MgAl<sub>1.998</sub>Mn<sub>0.002</sub>O<sub>4</sub> and then mixed with LiCl·H<sub>2</sub>O in a weight ratio of 1:5. The mixture was heated at 950 °C for 3 h. After cooling to room temperature, the product was washed with hot deionized water for 5 times to remove the salt, concentrated by centrifugation, and then dried at 100 °C for 12 h.